Microdosimetric Simulation of Gold-Nanoparticle Enhanced Radiotherapy

Maxim Azarkin *, Martin Kirakosyan, Vladimir Ryabov

Posted Date: 12 August 2024

doi: 10.20944/preprints202408.0778.v1

Keywords: gold nanoparticles; MC simulation; microdosimetry; radiosensitization mechanisms

Article

Microdosimetric Simulation of Gold-Nanoparticle Enhanced Radiotherapy

Maxim Azarkin *, Martin Kirakosyan and Vladimir Ryabov

P.N. Lebedev Physical Institute, 119991 Moscow , Russia
* Correspondence: azarkinmy@lebedev.ru (M. A.)

Abstract: Conventional X-ray therapy (XRT) is commonly applied to suppress cancerous tumors, however it often inflicts collateral damage to nearby healthy tissue. In order to provide a better conformity of the dose distribution in the irradiated tumor, proton therapy (PT) is increasingly being used to treat solid tumors. Furthermore, radiosensitization with gold nanoparticles (GNPs) has been extensively studied to increase the therapeutic ratio. The mechanism of radiosensitization is assumed to be connected with an enhancement of the absorbed dose due to huge photoelectric cross-sections with gold. Nevertheless, numerous theoretical studies mostly based on Monte Carlo (MC) simulations did not provide consistent and thorough picture of dose enhancement and, therefore, radiosensitization effect. Radiosensitization by nanoparticles in PT is even less studied than in XRT. Therefore, we investigate physics picture of GNP-enhanced RT using MC simulation with GEANT4 equipped with the most recent physics models, taking into account a wide range of physics processes relevant for realistic PT and XRT. Namely, we measured dose enhancement factors in the vicinity of GNP with diameters ranging from 10 nm to 80 nm. The dose enhancement in the vicinity of GNP reaches high values for XRT, while it is very modest for PT. The macroscopic dose enhancement factors for realistic therapeutic GNP concentrations are rather low for all RT scenarios, therefore other physicochemical and biological mechanisms should be additionally invoked for an explanation of the radiosensitization effect observed in many experiments.

Keywords: gold nanoparticles; MC simulation; microdosimetry; radiosensitization mechanisms

1. Introduction

Radiotherapy (RT) is an effective and widely used cancer treatment modality. Nevertheless, RT often inflicts collateral damage to nearby healthy tissue. A better targeting of tumors by RT is a compelling task for medical physicists. Modern RT achieved significant success using highly sophisticated apparatus to focus the radiation field to tumors for various beam types. To the advantage of the usage of proton and ion beams is a better targeting into the tumor over X-ray radiotherapy (XRT) due to a significant increase of deposited energy at the very end of the proton track, i.e. a well-known Bragg peak. In order to further increase therapeutic ratio, various radiosensitizers have been increasingly studied since 1960s [1,2]. A quite novel approach to this problem is the usage of radiosensitizing nanoparticles [3], i.e. particles with sizes varying from few nms to ≈ 100 nm. Such particles generally have increased ability to penetrate through blood vessels to surrounding tissue and show high cellular uptake [4]. In particular, nanoparticles, consisting of high-Z elements, are considered as dose enhancers due to huge photoelectric cross-sections at low photon energies that are proportional to Z^3–Z^5. The photoelectric processes can be followed by Auger electron emission. Produced electrons are soft (energy up to a few tens of keV) and have short absorption lengths in tissue that lead to a significant increase of the local dose deposition and ionization. Among heavy nanoparticles, gold nanoparticles are most widely studied due to their unique physico-chemical properties. Especially important for therapy are following properties: gold nanoparticles are easy to prepare, have controllable shape and size, allow easier surface binding for functionalization and a very high biocompatibility. Numerous studies demonstrate the increase of the effective absorbed dose in XRT with GNP both in vitro [5–7] and in vivo [8,9].

 doi:10.20944/preprints202408.0778.v1

Recently, the idea to use radiosensitizing nanoparticles also was extended to proton therapy (PT) and other types of nanopartilces with different radiosensitizing mechanisms [10–16]. Enhancement of PT with nanoparticles is especially tempting since it has a potential to dramatically decrease the damage to healthy tissue with respect to conventional XRT. Physics picture of proton beam interaction with tissue is different from XRT in many ways. Unlike XRT, irradiation by protons can induce nuclear reactions leading to production of neutrons, α-particles, unstable isotopes, and other products. Produced α-particles are of special interest since they have high linear energy transfer (LET) and, therefore, relative biological effectiveness (RBE). For that reason, a number of elements were suggested to enhance production of α-particles in tumors for PT [14,17,18]. However, recent in silico studies show that the enhancement of α-particle production is negligible at realistic therapeutic concentrations of boron-11, which has the largest proton fusion cross-section of α-particle production [19–21]. Electromagnetic ionization of protons with matter mostly depends on the density of the medium rather than Z of its atoms, which makes the advantage of heavy nanoparticles less evident. Nevertheless, in vitro [10,22–25] and in vivo [26,27] experiments show a significant radiosensitization effect in GNP-enhanced PT.

Contrary to nuclear processes [21], typical mean free paths of produced particles in electromagnetic interactions are at nanoscale, which is much less than the average distance between nanoparticles for therapeutic concentrations of GNPs. For that reason, an increase of dose deposition in the proximity of GNP can be one of the key effects relevant for the explanation of radiosensitization. Thus, in order to have a better picture of underlying mechanisms of the observed radiosensitizing effect induced by metallic nanoparticles under irradiation (XRT and PT), various studies based on Monte Carlo simulations have been undertaken[17,28–32]. These investigations were mainly focused on simulations of gamma-rays and proton-beams interactions with tissue-like (mostly water) systems with incorporated nanoparticles consisting of various materials at nanoscale. Thus, a significant increase of dose in the proximity of a nanoparticle was found for both X-rays and proton therapy. Some studies even went further and evaluated the production of reactive oxygen species around radiosensitizing nanoparticles [30,33]. However, current models of radiolysis are limited to production and propagation of a very few reactive species in pure water that is substantially different in its nature from the complex chemical and biological properties of the cytoplasm of a living cell. The above mentioned studies mostly consider simplified and idealistic systems where primary ionizing particles (beam) directly hit nanoparticles. There is a scarcity of full simulations that take into account the flux of secondary particles and realistic energy and spatial distribution of the incoming radiation field. Study of this kind was performed for XRT by Konefał et al. [34]. However, they did not use most recent discrete models of interactions of electrons in both, water and gold, and simulated irradiation by high-energy γ-rays only, i.e. 6 MV and 18 MV. One of the purposes of this work is to fill all of the above mentioned gaps.

In this study we simulate interactions of proton beam as well as 140kVp and 6MV X-rays with a gold nanoparticle (GNP) immersed in water using Monte Carlo simulation with GEANT4 11.2.1 [35]. To the advantage of this study is the usage of high-precision discrete models available in GEANT4. The simulation in water is performed using microscopic physical models for calculations of biological damage induced by ionizing radiation at DNA scale GEANT4-DNA [36,37]. To simulate the interactions of secondary electrons in GNP we use novel microscopic GEANT4_DNA_AU model [31,32]. Interaction of X-rays or proton beam with GNP and surrounding tissue is characterized with the dose enhancement factor (DEF) with respect to non-enhanced RT. In particular, we measure DEF as a function of a distance from the GNP center at microscopic scale. Also we calculate the macroscopic dose enhancement. Thanks to having the microscopic picture of a dose distribution, we are able to distinguish the energy deposited outside of GNP from the energy deposited inside a GNP. This approach has a significant impact on the macroscopic DEF in the living tissue and is applied for the first time.

This paper is organized as follows: results of the simulation are given in Sec. 2, the geometry of the simulated system, radiation fields, and physics models used are presented in Sec. 3, Sec. 4 discusses

 doi:10.20944/preprints202408.0778.v1

the nature of radiosensitizing effect in the light of obtained results and establishes connections of the results with various experimental data on NP-enhanced therapy, finally, Sec 5 summarizes our findings.

2. Results

We simulate irradiation of cubic tissue-like system with size of 20 cm by 140kVp and 6MV X-rays, and protons with energy of 95MeV. The layer located at depth from 5 cm to 7 cm represents cancerous tissue and loaded with spherical GNPs. The simulation is performed for GNP with diameter of 10 nm, 20 nm, 40 nm, 80 nm. Interaction of GNP with the 140kVp and 6 MVX-rays is studied only at depth of 7 cm, since the photon energy spectra have minor changes of their shape with depth. Energy of protons is adjusted so that Bragg peak position was at 7 cm, i.e. at the distal part of the tumor layer. The proton energy spectrum in frontal and distal parts of a tumor are very different, therefore both scenarios of interaction protons with the GNP are studied. It should be noted that large system size allowed to account secondary particles which also interact with GNP. The detailed description of geometry of stimulated system, radiation fields, and physics models used are given in Sec. 3. In the study we measure dose enhancement factor (DEF) as functions of a distance from the center of GNP that is defined as follows:

$$DEF(r) = \frac{D_{\mathrm{GNP}}(r)}{D_{\mathrm{WNP}}(r)}, \tag{1}$$

where $D_{\mathrm{GNP}}(r)$ is a dose as a function of a distance from the GNP center, $D_{\mathrm{WNP}}(r)$ is a dose as a function of a distance from water nanoparticle (WNP) which has the size of GNP and is placed at the same position. Both $D_{\mathrm{GNP}}(r)$ and $D_{\mathrm{WNP}}(r)$ are measured for the same fluxes of incoming radiation. Thus, $DEF(r)$ is a dose enhancement induced by the presence of GNP with respect to the scenario of a homogeneous water system.

These distributions are shown in Figure 1. It should be noted that for demonstrative purposes the DEF inside GNP is a ratio of spatial energy densities in GNP to WNP, i.e. it is higher than conventional DEF by a factor of 19.3 ($\rho_{\mathrm{Au}}/\rho_{\mathrm{H_2O}}$). The most prominent dose enhancement is, as expected, observed for irradiation by 140kVp X-rays for all particle sizes. In that case, the enhancement factor inside the GNP reaches $\approx 2 \times 10^3 - 3 \times 10^3$, while it drops to $\approx 2 \times 10^1$–10^2 in the first 5 nm scoring shell outside the GNP and then exponentially falls down reaching the pedestal. The enhancement increases with the GNP size. For instance, the enhancement is indistinguishable from the pedestal (difference is below few percent) at 80 nm, 150 nm, 250 nm, 450 nm for GNPs with sizes of 10 nm, 20 nm, 40 nm, 80 nm, respectively. Similar observations are qualitatively applied to the irradiation by 6MV X-rays, however dose enhancements in first shell around GNP are by a factor of ≈10 lower in comparison to the irradiation with 140kVp X-rays. The radii of enhanced dose zones are reduced to 50 nm, 80 nm, 150 nm, 250 nm for GNPs with sizes of 10 nm, 20 nm, 40 nm, 80 nm, respectively. In the case of irradiation by protons, the enhancement reaches a factor of 3 to 6 inside GNP and ≈ 2 in the first 5 nm shell outside the GNP and is negligible farther away. The enhancement is higher for a smaller GNP that can be explained by relatively higher yield of soft secondary electrons accompanying proton inside a smaller GNP to the contrary of a large one. The enhancement is also higher in frontal part of the tumor, since more energetic protons with higher probability interact with inner electrons of gold atoms. It should be noted that physics models of proton interaction with gold are not discrete. Hence, the production of δ-electrons inside GNP may be distorted if their energies are comparable or lower than the average ionization potential (i.e. 790 eV for gold). However, such soft electrons have a very short absorption lengths and may affect the dose deposition only within few nanometers outside of GNP

 doi:10.20944/preprints202408.0778.v1

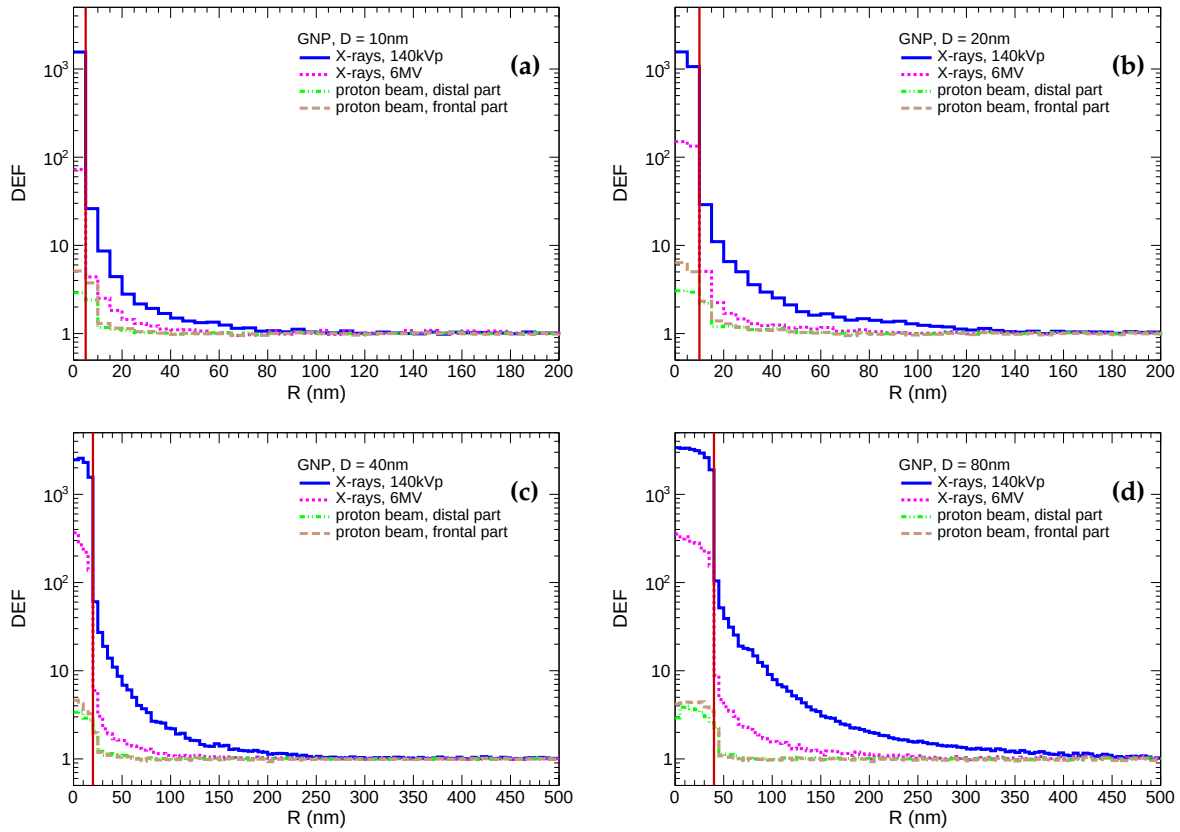

Figure 1. Dose enhancement factors (DEF) as a function of distance from the center of the gold nanopartice (GNP) immersed in a homogeneous water system. The DEF are measured for GNP with diameter of 10 nm (**a**), 20 nm (**b**), 40 nm (**c**), and 80 nm (**c**). The vertical red line marks GNP surface.

It should be noted that bare GNPs are mostly used for in vitro experiments. While in vivo experiments tend to use decorated GNP for functionalization. Most often, GNPs are coated by the polyethylene-glycol (PEG) or polyacreylic acid to achieve a better stability and biocompatibility. Furthermore, other ligands can be attached to the coated GNP to facilitate a selective delivery to the tumor. Thus, the decoration can increase the diameter of nanoparticles by up to another 20 nm. Given the fact that DEFs fall very steeply, the physical dose deposited in the living parts of cell is substantially reduced. This is especially important for GNP-enhanced PT, in which the dose enhancement is observed only in few nanometers outside of the GNP. Properties of the decoration can also be changed by a significantly increased ionization near the surface of a GNP, but this goes beyond the scope of this study.

The simulated dose enhancement in the vicinity of a GNP looks quite large for X-rays. Hence, it is instructive to assess the total dose enhancement due to GNP at macroscopic scale. Most of in vitro and in vivo studies of the radiosensitization effect use concentration of gold ranging from few mg/L to 100 mg/L [38]. In our study we set it to 10mg/L. This concentration gives an average distance between GNPs approximately 1 µm, 2 µm, 4 µm, and 8 µm for GNP sizes of 10 nm, 20 nm, 40 nm, 80 nm, respectively. Such a sparse distribution of GNPs means that most of tissue between them is not exposed to GNP induced radiation. It should be noted that the enhancement is present for X-rays since atoms of gold intercept some additional fraction of photons. The macroscopic dose enhancement is practically irrelevant for proton beam, since almost all protons are supposed to lose all their energy before distal side of the tumor anyway. Majority of studies of this kind evaluate macroscopic dose enhancement by integrating over entire volume, i.e. tissues and GNPs. In this study, using the microscopic picture of dose distribution, we assessed the macroscopic dose enhancement in the living tissue, excluding the GNP volumes. The approach is more relevant for the evaluation of dose enhancement effect on

 doi:10.20944/preprints202408.0778.v1

physicochemical and biological processes occurring in cells under irradiation. To quantify the dose enchantment at macroscopic scale, we use an additional relative dose (ARD) which is defined as follows:

$$ADR = \frac{D_{\mathrm{GNP}} - D_{\mathrm{W}}}{D_{\mathrm{W}}}, \tag{2}$$

where D_{W} is a dose deposited in pure water (i.e. non-enhanced RT) and D_{GNP} is a dose received in RT enhanced with GNP. The quantity is linear on concentration. The quantity measured in volume excluding GNP is denoted as ADR_{LT}, where "LT" stands for "living tissue". ADR_{LT} for different GNP sizes and radiation types are shown in Table 1. One can see that the ADR_{LT} decreases with the GNP size that can be explained by higher energy absorption for larger nanoparticles. For the sake of completeness, we also measured the percentage of ADR_{LT} in total ADR. It decreases with GNP size from approximately 25% to 15%. The absorption effect leads to dependency of ADR_{LT} on the particular spatial distribution of nanoparticles in cell. It varies from sparsely scattered one to clustered one. For the later, energy absorption inside nanoparticles may prove to be significantly higher if the average distance between nanoparticles would be of the order of hundred nanometers or less. It is worth mentioning, as experimental studies show, nanoparticles are often very densely packed in clusters inside lysosomes [39].

Table 1. Additional relative dose (ARD_{LT}) delivered to tumor due to the presence of GNP of different sizes at macroscopic scale. The dose is scored excluding GNP volume. The ARD is measured for GNP concentration in tissue of 10 mg/L.

Radiation Type	GNP Size			
	10 nm	20 nm	40 nm	80 nm
X-rays, 140kVp	2.4×10^{-4}	2.1×10^{-4}	1.9×10^{-4}	1.6×10^{-4}
X-rays, 6MV	3.5×10^{-5}	2.7×10^{-5}	2.3×10^{-5}	1.8×10^{-5}
proton beam	not applicable			

3. Methods and Models

3.1. Geometry of the Simulated System

The simulated system is represented by the cube with a side of 200 mm filled with a simplistic tissue-like material, which can be accessed in GEANT4 11 by calling the class `G4HumanPhantomMaterial` with the argument "*soft_tissue*". The material consists of a simple mixture of elements which comprise human soft tissue and has a density of human soft tissue. The proton beam or X-rays cross the cube perpendicularly to one of its faces, which is called frontal one. The layer located on depths between 50 mm and 70 mm with respect to the frontal face represents a malignant tumor. This layer contains a microscopic cubic water volume with the size of 1 mm placed at either frontal or distal sides of the tumor. The microscopic volume has a GNP in its center. We study interaction of radiation with GNP with the diameters of 10 nm, 20 nm, 40 nm and 80 nm. Two cases of different microscopic volume positions (either at the frontal or distal sides of the tumor) are considered for PT, since the proton energy significantly changes in the last 2 cm of its track (see Sec. 3.2). Differences of energy spectra of X-rays at the frontal and distal sides are minor, therefore only distal side is studied in the case of XRT. A layout of the simulated system is shown in Figure 2.

To conduct the study using reasonable computing resources, macroscopic and microscopic simulations of beam interactions are performed in two stages. On the first stage, proton beam and X-rays are passed through a thick layer of tissue in the geometric setting described above This provides energy spectrum of primary beam particles in the tumor region for the second stage of the simulation. On the second stage, modified beams interact with a microscopic system represented by the cube with a side of 1 mm with a GNP placed in its center. The size of the microscopic system is chosen so that most of secondary particles relevant for microdosimetric studies would be accounted, the 1 mm size is more than enough since a typical energy of secondaries is at most of order of $\sim$ keVs

 doi:10.20944/preprints202408.0778.v1

and have absorption lengths of no more than few micrometers. The simulation of a beam transport through the macroscopic tissue layer is performed using condensed history physics models, while the simulation of an irradiation of the microscopic region is performed using physics models dedicated for microdosimetric studies. Both approaches are described in details in Sec. 3.3.

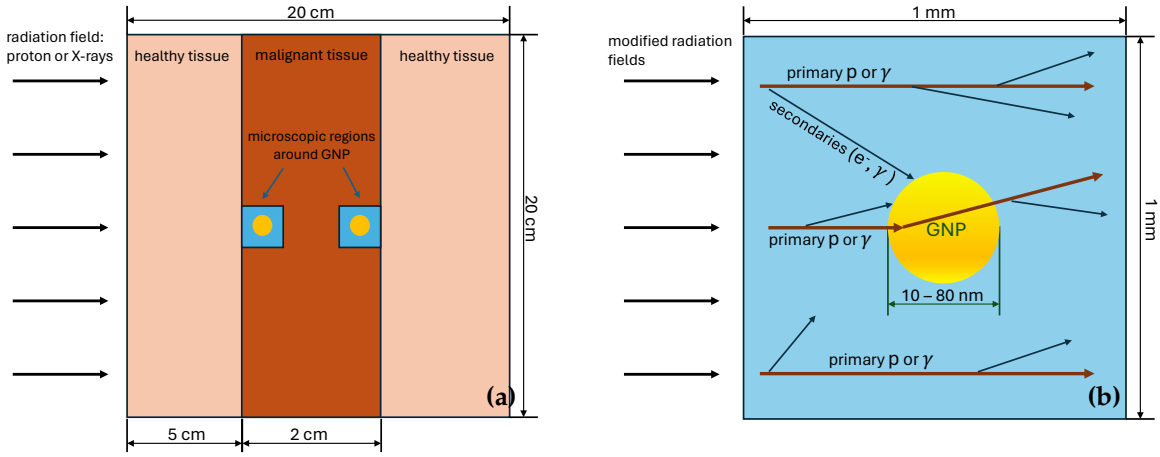

Figure 2. A schematic (not to scale) layout of the simulated system: **a**) The macroscopic setup represents a cube consisting of human soft tissue. The dark orange layer represents a tumor, smaller blue cubes represent the microscopic volume with a gold nanoparticle inside either on frontal or distal parts of the tumor layer. **b**) Close-up of a microscopic volume represents a water cube with a gold nanoparticles of various (10 to 80 nm) radii inside. Thick dark red arrows denote primary beam particles, thin black arrows indicate secondary particles that can interact with GNP as well.

3.2. Radiation Fields

The system is irradiated with a uniform flux of photons or protons. Energy spectra of incoming beam particles are chosen so that they would be close to realistic RT scenarios. Namely, we study an irradiation by X-rays with the 140kVp spectrum [40], 6MV photon beam [41], and a proton beam with the energy of 95 MeV. The chosen X-ray spectra are typical for modern CT and XRT machines. Energy of protons is adjusted so that Bragg peak is close to the distal part of the tumor layer that is demonstrated in Figure 3, which shows relative doses versus depth in tissue for both protons and X-rays. It is instructive to note that the doses deposited by both kilovoltage and megavoltage X-ray beams monotonically decrease from depth ≈10 mm and are undesirably high outside the tumor slice.

Energy distributions of photons and protons at the frontal side of the system and edges of the tumor layer for the corresponding beams are shown in Figure 4. These spectra of protons and photons at the frontal and distal sides of the tumor are used for irradiation of the microscopic system at the second simulation stage (see Sec. 3.3). One can see that energies of protons at depths of 5 cm and 7 cm are ≈ 45 MeV and of order of few MeVs, respectively. Therefore, the nature of proton interactions with tissue and incorporated GNP is expected to be different, and both scenarios are considered. Thus, for the sake of a clearer physical picture, we use both energy spectra for the simulation of irradiation of the microscopic system by protons. In real PT, the tumor is exposed to proton beam from different directions and with different energies for a better conformity and coverage of the tumor. Thus, the irradiation of different tumor parts is limited by these two cases. Conversely, the shape of energy spectra of both kilovoltage and megavoltage photons gradually changes with depths. The differences between frontal and distal sides of the tumor layer are minor, therefore we simulate irradiation of the microscopic system by X-rays only in the distal part of the tumor layer. However, it should be noted that for 6MV X-rays a fraction of the low-energy photons (E_γ <200 keV) significantly increases with depth. Such photons make a major contribution to the photoelectric effect for high-Z atoms. Therefore, the yield of corresponding physics processes and, hence, therapeutic outcome can be different for GNP-enhanced XRT of superficial and internal tumors.

Preprints.org (www.preprints.org) | NOT PEER-REVIEWED | Posted: 12 August 2024 doi:10.20944/preprints202408.0778.v1

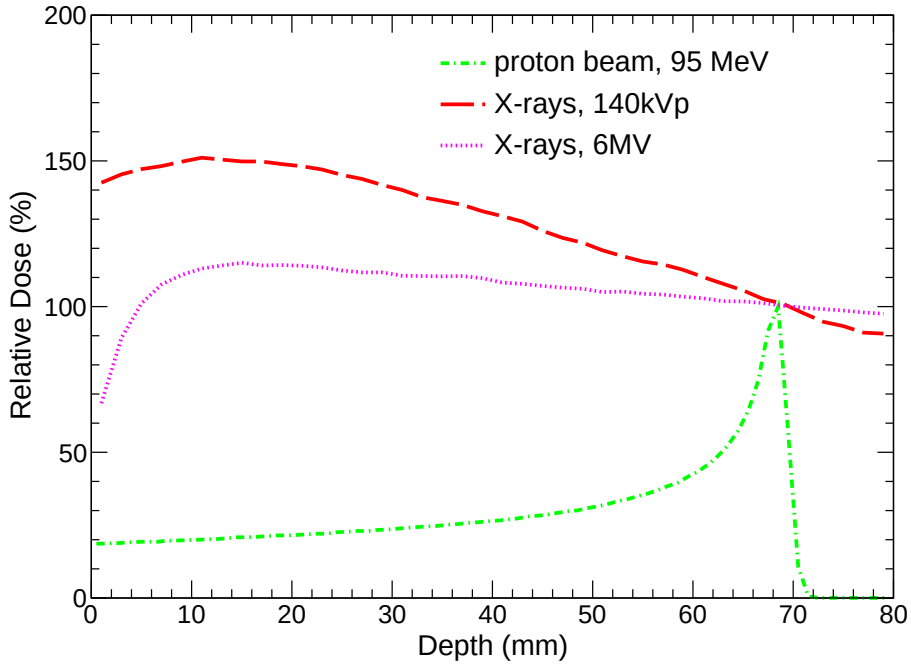

Figure 3. Relative dose versus tissue depth for different types of radiation.

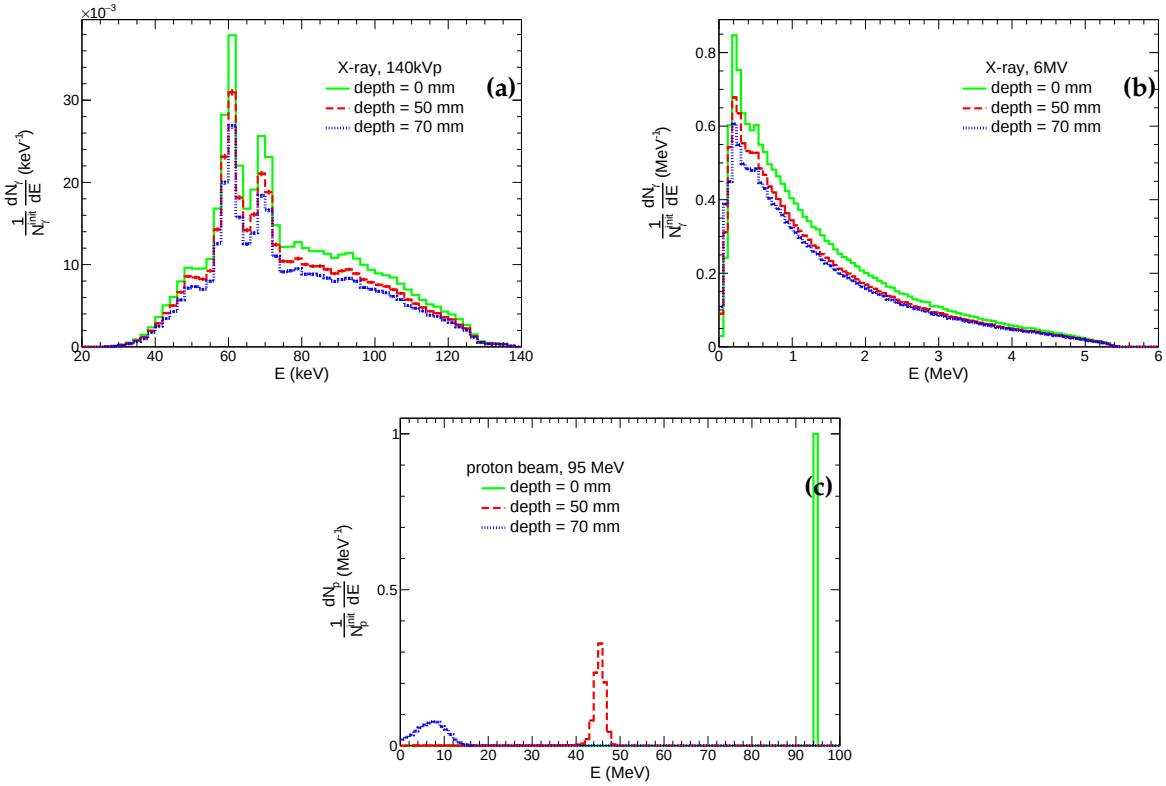

Figure 4. Energy distribution of 140kVp (**a**), 6MV (**b**) photons and protons (**c**) at different depths in tissue. These distributions are normalized by the number of initial beam photons ($N_{\gamma}^{\mathrm{init}}$) and protons ($N_{\mathrm{p}}^{\mathrm{init}}$).

 doi:10.20944/preprints202408.0778.v1

3.3. Physics Models

The aim of this study is an in silico investigation of patterns of the dose deposition in the vicinity of GNP for PT and XRT. The simulations is performed using an open source package for simulation of particle propagation in matter GEANT4 [35], version 11.2.1. Nowadays, GEANT4 is widely used in various fields of physics, from high energy and cosmo- physics to medicine. In GEANT4 approach, the user defines the geometry, physical processes and specific models for interaction of interested particles with a given media while GEANT4 Monte Carlo algorithms perform the simulation. The object-oriented nature of GEANT4 allows users to choose between models for different physical processes at various energy ranges. Wide range of physics models have been implemented for decades of development. Usually, a certain set of physical models is prepackaged to be used for particular simulation purposes. This sets are called physics lists. As mentioned in Sec. 3.1 our simulation setup has macroscopic and microscopic stages, both using dedicated physics models.

Let us briefly describe physics models used in our GEANT4 setup. The propagation of gamma and proton beams in macroscopic tissue layer is performed with QBBC physics list. For electromagnetic physics, QBBC uses a standard constructor `G4EmStandardPhysics_option0`. QBBC physics list also includes hadronic models for simulations of hadronic processes in tissue. Output spectra of primary beam particles from the macroscopic stage is used as an input for the next microscopic stage of the simulation. Thus, we simulate microscopic transportation of beam particles (namely, protons or gamma) and all secondaries through the microscopic volume, consisting of water, with a gold nanoparticle in its center. It should be said that water was chosen because the most advanced microscopic models in GEANT4 are available only for water among all other tissue-like materials. The particle transport inside the microscopic volume is performed with microscopic or discrete models in GEANT4 with maximum precision.

Namely, Livermore models are used for photon transport, i.e. photoelectric effect, gamma conversion, Compton and Reyleigh scattering. For proton and electron transport in water GEANT4-DNA set of models are used, while in gold recently implemented set of models for microscopic electron transport [31,32] were utilized. Unfortunately, at the moment discrete models for proton interaction in gold are not available. Thus, for proton transportation inside gold nanoparticle, standard GEANT4 models have been implemented for proton ionization, bremsstrahlung, electron-positron pair production and elastic scatterings. Since GEANT4 models for proton interaction in gold are not discrete and may distort energy loss of beam particles and production of low-energy secondaries. However, for the lack of a better option we use standard GEANT4 models for proton interactions with gold. Atomic deexitation processes (Auger electrons, Auger cascade, particle induced X-ray emission, fluorescence) are accounted by the use of GEANT4 G4UAtomicDeexcitation methods. Production cuts for gamma, electrons and protons were chosen to be 0.1 nm (low edge parameter – 1 eV). To switch between models in different GEANT4 regions "Sakata method" [31,32] from GEANT4 example `/extended/medical/dna/AuNP` was implemented.

More elaborately, to account for proton or gamma interactions with tissue on the macroscopic scale (see Figure 2 (**a**)) QBBC physics list is used. The spectra of protons and gamma after passing the thick layer (5 to 7 cm) of human soft tissue are used as an input for the main simulation code at nanoscale. The geometry at this stage consists of 2 microscopic regions, as represented on Figure 2 (**b**):

Region 1) the 1 millimeter cube of water to account for production of secondaries.

Region 2) Gold nanoparticle of various radii inside the cell.

In these microscopic regions Livermore models are being used for photon-gold interactions. For electrons and protons, physics models depend on the region.

Specifically, following set of models is used for electrons:

- in water region, GEANT4-DNA models are implemented
- in GNP region, a new set of GEANT4-DNA discrete models for electron interaction with gold [31];

while for protons:

 doi:10.20944/preprints202408.0778.v1

– in water region, GEANT4-DNA models are implemented
– in GNP region, standard GEANT4 models are being used for lack of a better option.

4. Discussion

The macroscopic dose enhancement is small or even negligible for realistic therapeutic concentrations of gold nanoparticles for all kinds of RT. Dose enhancement in the vicinity of GNP is quite high for X-rays in kilovoltage energy range and still significant for megavoltage X-rays. By contrast, proton therapy demonstrates a very modest enhancement observed in the very close proximity of the GNP. Nevertheless, in vitro [22–24] and in vivo [26] experiments show a significant radiosensitization effect in GNP-enhanced PT. Moreover, elements with low and moderate Z also proved to be effective at radiosensitizing PT. For instance, nanoparticles consisting of TiO_2, ZnO, Sodium Mercaptododecaborate etc. have shown significant radiosensitizing effect [42–44]. All these facts indicate that multiple mechanisms should be involved.

It is generally accepted that RT results in increased production of reactive oxygen species (ROS), causing oxidative stress and triggering apoptosis. A number of recent studies of GNP-enhanced (and some other NPs) radiotherapy strongly indicates an increased production of ROS with respect to the non-enhanced one. Physico-chemical GNP-related mechanisms that facilitate the increase of ROS generation in cells are GNP-enhanced radiolysis and radiation-induced catalytic enhancement of ROS production. The former is proportional to dose enhancement, at least according to known mechanisms of radiolysis [33], and proved to be small on macroscopic scales, whereas the latter ought to have a huge enhancement factor to be viable of causing observed radiosensitization. It is established that electrically active surface of GNPs and thier high surface to volume ratio may provide catalyzation of chemical reactions [45]. Ionzing radiation is assumed to enhance the catalytic property of ROS generation by production of additional donor electrons [46]. Low work function can further facilitate these processes [47]. It should be noted that radiation-enhanced catalysis takes effect during the physical stage of interaction of ionizing radiation with nanoparticles at very short time scales. Unfortunately, as far as authors are concerned, there are still neither theoretical nor MC-based quantitative estimations of the radiation-induced catalytic enhancement factor based on first principles. It is worth mentioning that catalytic properties may also be tightly conjugated with the functionalization [48] making the process of ROS production even more complex. Thus, it is still not clear whether catalysis may cause few orders of enhancement needed for the explanation of observed sensitization by GNPs.

Another radiosensitization mechanism may be connected with the acquisition of a positive charge by NP via ionization caused by radiation [49,50]. It is generally accepted that positively charged NPs have higher cellular uptake and cytotoxicity than neutral or negative ones [38,51–53]. It was found that positively charged GNPs can cause oxidative stress, interfere with the cell signaling system, and inhibit DNA reparation [52,53]. The observations show that most kinds of NPs have surface charges from -30mV to +30mV, whereas NPs with surface charge of >20mV demonstrate an acute cytotoxic effect[48,54]. The long-range displacement of electrons from the nanoparticle by irradiation can significantly alter potential at its surface, making it more cytotoxic. For instance, the potential of spherical system is given by the formula:

$$\phi(r) = \frac{Q}{4\pi\varepsilon_0 r}, \tag{3}$$

where Q is a total charge of the system, r is a distance from the center of the system, ε_0 is the vacuum electric permittivity. For example, a single displaced electron from a GNP with the size of 20 nm can add the following electric potential at its surface: $\phi(20\,\mathrm{nm}) = 1.6 \cdot 10^{-19}\mathrm{C}/(4\pi \cdot 8.9 \cdot 10^{-12}\mathrm{F} \cdot \mathrm{m}^{-1} \cdot 20 \cdot 10^{-9}\mathrm{m}) \approx 75\,\mathrm{mV}$. Obviously, electron yield from the surface of a nanoparticle goes in parallel with the opposite process of the capture of free electrons from the medium. In the end, the kinetic interplay between these two processes and their time scales determines the resulting electric charges of nanoparticles in media and their dependence on time. The above-mentioned kinetic is not

 doi:10.20944/preprints202408.0778.v1

sufficiently investigated at the moment for different types of nanoparticles neither experimentally nor theoretically. Nevertheless, one can cautiously assume that the acquired charge may be non-negligible on macroscopic time scales in cell environment.

Effect of this kind was observed for TiO_2 nanoparticles irradiated UV light [55,56]. Photoexcited electrons were emitted from nanoparticles to surrounding bulk and increased Z-potential of the nanoparticle. It is of special importance that the change of surface charge was persistent over time. The persistence of increased charge of the surface came up in in vitro experiments [56,57]. Thus, nanoparticles pre-exposed to UV light decreased cell viability in comparison to pristine nanoparticles. One should note these studied reported that pre-exposed nanoparticles did not increase ROS level and did not cause an oxidative stress.

The above discussed physical and physico-chemical mechanisms are followed by various biological processes. It is argued that sensitization to radiation can happen due to biological mechanism triggered by GNP prior to irradiation. For instance, it was found that GNPs can bind endogenous antioxidants inside cells making them vulnerable to radiation. Moreover, it was shown that GNPs cause ROS production via inhibition of thioredoxin reductase 1 and other redox-relevant mechanisms (see [58] and references therein). While these effects are beyond the scope of this study, however, it is natural to assume that biological GNP-induced and radiation-induced processes can be synergistic in NP-enhanced RT.

All in all, large photoelectric cross-sections of gold result in hugely increased ionization in the very close proximity to GNP and may serve as an initial seed to increase the charge of nanoparticles in XRT, especially at kilovoltage energies. Interaction of protons with atoms of gold results in insignificant increase of the local dose deposition, therefore mechanisms of the observed radiosensitization is connected to the soft energy physico-chemical processes. In conclusion, various physico-chemical (e.g.catalysis of ROS generation) and biological mechanisms ought to be invoked for the explanation of observed radiosensitization effect in all kinds of RT.

5. Conclusions

In this study we obtained the dose enhancement factors in tissue in the vicinity of GNPs using Monte Carlo simulations with GEANT4 11.2.1 and most recent discrete models of particle tracking in liquid water and gold for three types of radiation: proton beam, kilovoltage and megavoltage X-rays. The dose enhancement factors were measured for spherical GNPs with diameters of 10 nm, 20 nm, 40 nm, and 80 nm. It is worth mentioning that the simulation took in into account effects of the beam passage to the tumor through thick tissue layers, including interaction of secondary particles with a GNP.

The most prominent dose enhancement is observed for 140kVp X-rays. Thus, dose enhancement factor in the first 5-nm shell outside GNP increases with its size from $\approx 3 \times 10^1$ to $\approx 10^2$, whereas it falls down close to unity at distances of 80 nm, 150 nm, 250 nm, 450 nm for GNPs with the sizes of 10 nm, 20 nm, 40 nm, 80 nm, respectively. The shape of DEF profiles for 6MV X-Rays are close 140kVp X-rays, however values of DEFs are one order lower compared to 140kVp X-rays, and dose enhancement zones are nearly 2 times smaller for all GNP sizes. The dose enhancement factor for proton beam is ≈ 2 in the first 5-nm shell outside of a GNP, whereas it is negligible further away from the GNP surface.

The dose enhancement in the proximity of GNP for XRT turns out to be very high, while the macroscopic dose enhancements are still negligible for realistic therapeutic concentrations of GNPs in tissue. Therefore, modification of surface charge and other physico-chemical properties of the GNPs ought to play a major role in the sensitization process. The increased level of ROS is considered to be one of the main reasons of the decrease in the survival of cells exposed to radiation. The yield of produced ROS is expected to be proportional to a dose enhancement factor. Given a small dose enhancement for all types of radiation at realistic GNP concentrations, it becomes clear that other radiation-induced mechanisms of ROS generation should be involved. Hence, enhanced ROS

 doi:10.20944/preprints202408.0778.v1

production can be connected to nanoparticle-mediated biological redox processes. It should be noted that there is evidence that NP can reduce cell survival without enhanced ROS production, suggesting that other biochemical mechanisms may come into play. The radiosensitization in PT almost certainly caused neither local dose enchantment nor related ROS production in the physical stage of irradiation, and the biological processes should play a major role here.

Funding: This work was supported by the Ministry of Science and Higher Education of Russia within the Agreement no. 075-15-2021-1347.

Institutional Review Board Statement: Not applicable

Informed Consent Statement: Not applicable

Data Availability Statement: The code used for simulations presented in this study is available upon request to authors.

Conflicts of Interest: The authors declare no conflict of interest.

Abbreviations

The following abbreviations are used in this manuscript:

MDPI	Multidisciplinary Digital Publishing Institute
DOAJ	Directory of open access journals
TLA	Three letter acronym
LD	Linear dichroism

References

1. Gong, L.; Zhang, Y.; Liu, C.; Zhang, M.; Han, S. Application of radiosensitizers in cancer radiotherapy. *Int. J. Nanomedicine* **2021**, *16*, 1083–1102.
2. Moulder, J.E. Chemical radiosensitizers: the Journal history. *International Journal of Radiation Biology* **2019**, *95*, 940–944. https://doi.org/10.1080/09553002.2019.1569779.
3. Kwatra, D.; Venugopal, A.; Anant, S. Nanoparticles in radiation therapy: a summary of various approaches to enhance radiosensitization in cancer. *Translational Cancer Research* **2013**, *2*. https://doi.org/10.3978/j.issn.2218-676X.2013.08.06.
4. Augustine, R.; Hasan, A.; Primavera, R.; Wilson, R.J.; Thakor, A.S.; Kevadiya, B.D. Cellular uptake and retention of nanoparticles: Insights on particle properties and interaction with cellular components. *Materials Today Communications* **2020**, *25*, 101692. https://doi.org/https://doi.org/10.1016/j.mtcomm.2020.101692.
5. Kong, T.; Zeng, J.; Wang, X.; Yang, X.; Yang, J.; McQuarrie, S.; McEwan, A.; Roa, W.; Chen, J.; Xing, J.Z. Enhancement of Radiation Cytotoxicity in Breast-Cancer Cells by Localized Attachment of Gold Nanoparticles. *Small*, *4*, 1537–1543. https://doi.org/10.1002/smll.200700794.
6. Zhang, X.D.; Wu, D.; Shen, X.; Chen, J.; Sun, Y.M.; Liu, P.X.; Liang, X.J. Size-dependent radiosensitization of PEG-coated gold nanoparticles for cancer radiation therapy. *Biomaterials* **2012**, *33*, 6408–6419. https://doi.org/10.1016/j.biomaterials.2012.05.047.
7. Soares, S.; Faria, I.; Aires, F.; Monteiro, A.; Pinto, G.; Sales, M.G.; Correa-Duarte, M.A.; Guerreiro, S.G.; Fernandes, R. Application of Gold Nanoparticles as Radiosensitizer for Metastatic Prostate Cancer Cell Lines. *International Journal of Molecular Sciences* **2023**, *24*. https://doi.org/10.3390/ijms24044122.
8. Hainfeld, J.F.; Slatkin, D.N.; Smilowitz, H.M. The use of gold nanoparticles to enhance radiotherapy in mice. *Physics in Medicine Biology* **2004**, *49*, N309. https://doi.org/10.1088/0031-9155/49/18/N03.
9. Hainfeld, J.F.; Smilowitz, H.M.; O'Connor, M.J.; Dilmanian, F.A.; Slatkin, D.N. Gold Nanoparticle Imaging and Radiotherapy of Brain Tumors in Mice. *Nanomedicine* **2013**, *8*, 1601–1609. https://doi.org/10.2217/nnm.12.165.
10. Cunningham, C.; de Kock, M.; Engelbrecht, M.; Miles, X.; Slabbert, J.; Vandevoorde, C. Radiosensitization Effect of Gold Nanoparticles in Proton Therapy. *Front Public Health* **2021**, *9*, 699822. https://doi.org/https://doi.org/10.3389/fpubh.2021.699822.

11. Porcel, E.; Liehn, S.; Remita, H.; Usami, N.; Kobayashi, K.; Furusawa, Y.; Sech, C.L.; Lacombe, S. Platinum nanoparticles: a promising material for future cancer therapy? *Nanotechnology* **2010**, *21*, 085103. https://doi.org/10.1088/0957-4484/21/8/085103.
12. Briggs, A.; Corde, S.; Oktaria, S.; Brown, R.; Rosenfeld, A.; Lerch, M.; Konstantinov, K.; Tehei, M. Cerium oxide nanoparticles: influence of the high-Z component revealed on radioresistant 9L cell survival under X-ray irradiation. *Nanomedicine: Nanotechnology, Biology and Medicine* **2013**, *9*, 1098–1105. https://doi.org/10.1016/j.nano.2013.02.008.
13. Brown, R.; Tehei, M.; Oktaria, S.; Briggs, A.; Stewart, C.; Konstantinov, K.; Rosenfeld, A.; Corde, S.; Lerch, M. High-Z Nanostructured Ceramics in Radiotherapy: First Evidence of Ta2O5-Induced Dose Enhancement on Radioresistant Cancer Cells in an MV Photon Field. *Particle & Particle Systems Characterization*, *31*, 500–505. https://doi.org/10.1002/ppsc.201300276.
14. Bláha, P.; Feoli, C.; Agosteo, S.; Calvaruso, M.; Cammarata, F.P.; Catalano, R.; Ciocca, M.; Cirrone, G.A.P.; Conte, V.; Cuttone, G.; et al. The Proton-Boron Reaction Increases the Radiobiological Effectiveness of Clinical Low- and High-Energy Proton Beams: Novel Experimental Evidence and Perspectives. *Frontiers in Oncology* **2021**, *11*. https://doi.org/10.3389/fonc.2021.682647.
15. Roy, I.; Krishnan, S.; Kabashin, A.V.; Zavestovskaya, I.N.; Prasad, P.N. Transforming Nuclear Medicine with Nanoradiopharmaceuticals. *ACS Nano* **2022**, *16*, 5036–5061. https://doi.org/10.1021/acsnano.1c10550.
16. Zavestovskaya, I.N.; Popov, A.L.; Kolmanovich, D.D.; Tikhonowski, G.V.; Pastukhov, A.I.; Savinov, M.S.; Shakhov, P.V.; Babkova, J.S.; Popov, A.A.; Zelepukin, I.V.; et al. Boron Nanoparticle-Enhanced Proton Therapy for Cancer Treatment. *Nanomaterials* **2023**, *13*. https://doi.org/10.3390/nano13152167.
17. Tabbakh, F.; Hosmane, N.S.; Tajudin, S.M.; Ghorashi, A.H.; Morshedian, N. Using 157Gd doped carbon and 157GdF4 nanoparticles in proton-targeted therapy for effectiveness enhancement and thermal neutron reduction: a simulation study. *Scientific Reports* **2022**, *12*, 17404. https://doi.org/10.1038/s41598-022-22429-0.
18. Shahmohammadi Beni, M.; Islam, M.R.; Kim, K.M.; Krstic, D.; Nikezic, D.; Yu, K.N.; Watabe, H. On the effectiveness of proton boron fusion therapy (PBFT) at cellular level. *Scientific Reports* **2022**, *12*, 18098. https://doi.org/10.1038/s41598-022-23077-0.
19. Chiniforoush, T.A.; Hadadi, A.; Kasesaz, Y.; Sardjono, Y. Evaluation of effectiveness of equivalent dose during proton boron fusion therapy (PBFT) for brain cancer: A Monte Carlo study. *Appl Radiat Isot* **2021**, *170*, 109596. https://doi.org/10.1016/j.apradiso.2021.109596.
20. Bagulya, A.V.; Grichine, V.M.; Zavestovskaya, I.N.; Ryabov, V.A. Geant4 Simulation of p + ^{11}B $\rightarrow$ 3α reaction. *BULLETIN OF THE LEBEDEV PHYISICS INSTITUTE* **2023**, pp. 27–35. https://doi.org/10.3103/S1068335623040036.
21. Azarkin, M.; Kirakosyan, M.; Ryabov, V. Study of Nuclear Reactions in Therapy of Tumors with Proton Beams. *International Journal of Molecular Sciences* **2023**, *24*. https://doi.org/10.3390/ijms241713400.
22. Liu, C.J.; Wang, C.H.; Chen, S.T.; Chen, H.H.; Leng, W.H.; Chien, C.C.; Wang, C.L.; Kempson, I.M.; Hwu, Y.; Lai, T.C.; et al. Enhancement of cell radiation sensitivity by pegylated gold nanoparticles. *Physics in Medicine and Biology* **2010**, *55*, 931–945. https://doi.org/10.1088/0031-9155/55/4/002.
23. Polf, J.C.; Bronk, L.F.; Driessen, W.H.P.; Arap, W.; Pasqualini, R.; Gillin, M. Enhanced relative biological effectiveness of proton radiotherapy in tumor cells with internalized gold nanoparticles. *Appl. Phys. Lett.* **2011**, *98*, 193702. https://doi.org/10.1063/1.3589914.
24. Li, S.; Penninckx, S.; Karmani, L.; Heuskin, A.C.; Watillon, K.; Marega, R.; Zola, J.; Corvaglia, V.; Genard, G.; Gallez, B.; et al. LET-dependent radiosensitization effects of gold nanoparticles for proton irradiation. *Nanotechnology* **2016**, *27*, 455101. https://doi.org/10.1088/0957-4484/27/45/455101.
25. Lo, C.Y.; Tsai, S.W.; Niu, H.; Chen, F.H.; Hwang, H.C.; Chao, T.C.; Hsiao, I.T.; Liaw, J.W. Gold-Nanoparticles-Enhanced Production of Reactive Oxygen Species in Cells at Spread-Out Bragg Peak under Proton Beam Radiation. *ACS Omega* **2023**, *8*, 17922–17931. https://doi.org/10.1021/acsomega.3c01025.
26. Kim, J.K.; Seo, S.J.; Kim, H.T.; Kim, K.H.; Chung, M.H.; Kim, K.R.; Ye, S.J. Enhanced proton treatment in mouse tumors through proton irradiated nanoradiator effects on metallic nanoparticles. *Physics in Medicine and Biology* **2012**, *57*, 8309. https://doi.org/10.1088/0031-9155/57/24/8309.
27. Wolfe, T.; Grant, J.; Wolfe, A.; Gillin, M.; Krishnan, S. WE-G-BRE-07: Proton Therapy Enhanced by Tumor-Targeting Gold Nanoparticles: A Pilot in Vivo Experiment at The Proton Therapy Center at MD Anderson Cancer Center. *Medical Physics*, *41*, 518–518. https://doi.org/https://doi.org/10.1118/1.4889482.

 doi:10.20944/preprints202408.0778.v1

28. McKinnon, S.; Guatelli, S.; Incerti, S.; Ivanchenko, V.; Konstantinov, K.; Corde, S.; Lerch, M.; Tehei, M.; Rosenfeld, A. Local dose enhancement of proton therapy by ceramic oxide nanoparticles investigated with Geant4 simulations. *Physica Medica* **2016**, *32*, 1584–1593. https://doi.org/10.1016/j.ejmp.2016.11.112.
29. Martínez-Rovira, I.; Prezado, Y. Evaluation of the local dose enhancement in the combination of proton therapy and nanoparticles. *Medical Physics*, *42*, 6703–6710. https://doi.org/10.1118/1.4934370.
30. Tran, H.; Karamitros, M.; Ivanchenko, V.; Guatelli, S.; McKinnon, S.; Murakami, K.; Sasaki, T.; Okada, S.; Bordage, M.; Francis, Z.; et al. Geant4 Monte Carlo simulation of absorbed dose and radiolysis yields enhancement from a gold nanoparticle under MeV proton irradiation. *Nuclear Instruments and Methods in Physics Research Section B: Beam Interactions with Materials and Atoms* **2016**, *373*, 126–139. https://doi.org/10.1016/j.nimb.2016.01.017.
31. Sakata, D.; Kyriakou, I.; Okada, S.; Tran, H.N.; Lampe, N.; Guatelli, S.; Bordage, M.C.; Ivanchenko, V.; Murakami, K.; Sasaki, T.; et al. Geant4-DNA track-structure simulations for gold nanoparticles: The importance of electron discrete models in nanometer volumes. *Physica medica* **2018**, *45*, 2230–2242. https://doi.org/10.1002/mp.12827.
32. Sakata, D.; Kyriakou, I.; Tran, H.N.; Bordage, M.C.; Rosenfeld, A.; Ivanchenko, V.; Incerti, S.; Emfietzoglou, D.; Guatelli, S. Electron track structure simulations in a gold nanoparticle using Geant4-DNA. *Physica medica* **2019**, *63*, 98–104. https://doi.org/10.1016/j.ejmp.2019.05.023.
33. Peukert, D.; Kempson, I.; Douglass, M.; Bezak, E. Gold Nanoparticle Enhanced Proton Therapy: Monte Carlo Modeling of Reactive Species' Distributions Around a Gold Nanoparticle and the Effects of Nanoparticle Proximity and Clustering. *International Journal of Molecular Sciences* **2019**, *20*. https://doi.org/10.3390/ijms20174280.
34. Konefał, A.; Lniak, W.; Rostocka, J.; Orlef, A.; Sokół, M.; Kasperczyk, J.; Jarząbek, P.; Wrońska, A.; Rusiecka, K. Influence of a shape of gold nanoparticles on the dose enhancement in the wide range of gold mass concentration for high-energy X-ray beams from a medical linac. *Reports of Practical Oncology & Radiotherapy* **2020**, *25*, 579–585. https://doi.org/10.1016/j.rpor.2020.05.003.
35. Agostinelli, S.; Allison, J.; Amako, K.; Apostolakis, J.; Araujo, H.; Arce, P.; Asai, M.; Axen, D.; Banerjee, S.; Barrand, G.; et al. Geant4—a simulation toolkit. *Nuclear Instruments and Methods in Physics Research Section A: Accelerators, Spectrometers, Detectors and Associated Equipment* **2003**, *506*, 250–303. https://doi.org/10.1016/S0168-9002(03)01368-8.
36. Incerti, S.; Baldacchino, G.; Bernal, M.; Capra, R.; Champion, C.; Fransis, Z.; Guèye, P.; Mantero, A.; Mascialino, B.; Moretto, P.; et al. The Geant4-DNA project. *International Journal of Modeling, Simulation, and Scientific Computing* **2010**, *01*, 157–178. https://doi.org/10.1142/S1793962310000122.
37. Geant4-DNA collaboration. Geant4-DNA : Extending the Geant4 Monte Carlo simulation toolkit for radiobiology. Available online: http://geant4-dna.org.
38. Chen, Y.; Yang, J.; Fu, S.; Wu, J. Gold nanoparticles as radiosensitizers in cancer radiotherapy. *International Journal of Nanomedicine* **2020**, *15*, 9407–9430. https://doi.org/10.2147/IJN.S272902.
39. Piccolo, O.; Lincoln, J.D.; Melong, N.; Orr, B.C.; Fernandez, N.R.; Borsavage, J.; Berman, J.N.; Robar, J.; Ha, M.N. Radiation dose enhancement using gold nanoparticles with a diamond linear accelerator target: a multiple cell type analysis. *Scientific Reports* **2022**, *12*, 1559. https://doi.org/10.1038/s41598-022-05339-z.
40. Duan, X.; Wang, J.; Yu, L.; Leng, S.; McCollough, C.H. CT scanner x-ray spectrum estimation from transmission measurements. *Medical Physics* **2011**, *38*, 993–997. https://doi.org/10.1118/1.3547718.
41. Brualla, L.; Rodriguez, M.; Sempau, J.; Andreo, P. PENELOPE/PRIMO-calculated photon and electron spectra from clinical accelerators. *Radiation Oncology* **2019**, *14*, 6. https://doi.org/10.1186/s13014-018-1186-8.
42. Morita, K.; Nishimura, Y.; Nakamura, S.; Arai, Y.; Numako, C.; Sato, K.; Nakayama, M.; Akasaka, H.; Sasaki, R.; Ogino, C.; et al. Titanium oxide nano-radiosensitizers for hydrogen peroxide delivery into cancer cells. *Colloids and Surfaces B: Biointerfaces* **2021**, *198*, 111451. https://doi.org/10.1016/j.colsurfb.2020.111451.
43. Meyer, T.J.; Scherzad, A.; Moratin, H.; Gehrke, T.E.; Killisperger, J.; Hagen, R.; Wohlleben, G.; Polat, B.; Dembski, S.; Kleinsasser, N.; et al. The Radiosensitizing Effect of Zinc Oxide Nanoparticles in Sub-Cytotoxic Dosing Is Associated with Oxidative Stress In Vitro. *Materials (Basel)* **2019**, *12*. https://doi.org/10.3390/ma12244062.

44. Bláha, P.; Feoli, C.; Agosteo, S.; Calvaruso, M.; Cammarata, F.P.; Catalano, R.; Ciocca, M.; Cirrone, G.A.P.; Conte, V.; Cuttone, G.; et al. The Proton-Boron Reaction Increases the Radiobiological Effectiveness of Clinical Low- and High-Energy Proton Beams: Novel Experimental Evidence and Perspectives. *Front Oncol* **2021**, *11*, 682647. https://doi.org/DOI:10.3389/fonc.2021.682647.
45. Bano, A.; Dawood, A.; Saira, F.; Malik, A.; Alkholief, M.; Ahmad, H.; Khan, M.A.; Ahmad, Z.; Bazighifan, O. Enhancing catalytic activity of gold nanoparticles in a standard redox reaction by investigating the impact of AuNPs size, temperature and reductant concentrations. *Scientific Reports* **2023**, *13*, 12359. https://doi.org/10.1038/s41598-023-38234-2.
46. Penninckx, S.; Heuskin, A.C.; Michiels, C.; Lucas, S. Gold Nanoparticles as a Potent Radiosensitizer: A Transdisciplinary Approach from Physics to Patient. *Cancers* **2020**, *12*. https://doi.org/10.3390/cancers12082021.
47. Kessler, A.; Hedberg, J.; Blomberg, E.; Odnevall, I. Reactive Oxygen Species Formed by Metal and Metal Oxide Nanoparticles in Physiological Media—A Review of Reactions of Importance to Nanotoxicity and Proposal for Categorization. *Nanomaterials* **2022**, *12*. https://doi.org/10.3390/nano12111922.
48. Sun, H.; Jiang, C.; Wu, L.; Bai, X.; Zhai, S. Cytotoxicity-Related Bioeffects Induced by Nanoparticles: The Role of Surface Chemistry. *Frontiers in Bioengineering and Biotechnology* **2019**, *7*. https://doi.org/10.3389/fbioe.2019.00414.
49. Verkhovtsev, A.V.; Korol, A.V.; Solov'yov, A.V. Revealing the Mechanism of the Low-Energy Electron Yield Enhancement from Sensitizing Nanoparticles. *Phys. Rev. Lett.* **2015**, *114*, 063401. https://doi.org/10.1103/PhysRevLett.114.063401.
50. Zygmanski, P.; Sajo, E.; Brivio, D. Nanoparticle-based radiotherapy: Is dose all that matters? *Z Med Phys* **2023**, *33*, 119–122. https://doi.org/10.1016/j.heliyon.2023.e17252.
51. Her, S.; Jaffray, D.A.; Allen, C. Gold nanoparticles for applications in cancer radiotherapy: Mechanisms and recent advancements. *Advanced Drug Delivery Reviews* **2017**, *109*, 84–101. Radiotherapy for cancer: present and future, https://doi.org/https://doi.org/10.1016/j.addr.2015.12.012.
52. Schaeublin, N.M.; Braydich-Stolle, L.K.; Schrand, A.M.; Miller, J.M.; Hutchison, J.; Schlager, J.J.; Hussain, S.M. Surface charge of gold nanoparticles mediates mechanism of toxicity. *Nanoscale* **2011**, *3*, 410–420. https://doi.org/10.1039/C0NR00478B.
53. May, S.; Hirsch, C.; Rippl, A.; Bohmer, N.; Kaiser, J.P.; Diener, L.; Wichser, A.; Bürkle, A.; Wick, P. Transient DNA damage following exposure to gold nanoparticles. *Nanoscale* **2018**, *10*, 15723–15735. https://doi.org/10.1039/C8NR03612H.
54. Adabi, M.; Naghibzadeh, M.; Adabi, M.; Zarrinfard, M.A.; Esnaashari, S.S.; Seifalian, A.M.; Faridi-Majidi, R.; Tanimowo Aiyelabegan, H.; Ghanbari, H. Biocompatibility and nanostructured materials: applications in nanomedicine. *Artif Cells Nanomed Biotechnol* **2016**, *45*, 833–842. https://doi.org/10.1080/21691401.2016.1178134.
55. Sun, J.; Guo, L.H.; Zhang, H.; Zhao, L. UV irradiation induced transformation of TiO2 nanoparticles in water: aggregation and photoreactivity. *Environmental Science & Technology* **2014**, *48*, 11962–11968. https://doi.org/10.1021/es502360c.
56. Kose, O.; Tomatis, M.; Turci, F.; Belblidia, N.B.; Hochepied, J.F.; Pourchez, J.; Forest, V. Short Preirradiation of TiO(2) Nanoparticles Increases Cytotoxicity on Human Lung Coculture System. *Chemical Research in Toxicology* **2021**, *34*, 733–742. https://doi.org/10.1021/acs.chemrestox.0c00354.
57. Petković, J.; Küzma, T.; Rade, K.; Novak, S.; Filipič, M. Pre-irradiation of anatase TiO2 particles with UV enhances their cytotoxic and genotoxic potential in human hepatoma HepG2 cells. *Journal of Hazardous Materials* **2011**, *196*, 145–152. https://doi.org/10.1016/j.jhazmat.2011.09.004.
58. Rosa, S.; Connolly, C.; Schettino, G.; Butterworth, K.T.; Prise, K.M. Biological mechanisms of gold nanoparticle radiosensitization. *Cancer Nanotechnology* **2017**, *8*, 2. https://doi.org/10.1186/s12645-017-0026-0.